Electronic Supplementary Material (ESI) for Physical Chemistry Chemical Physics

Supporting Information Available

Connecting theory with experiment to understand the initial nucleation steps of heteropolyoxometalate clusters

Laia Vilà-Nadal, Scott G. Mitchel, Antonio Rodríguez-Fortea, Haralampos N. Miras,

Leroy Cronin and Josep M. Poblet

Index

Table S1. Reaction energies (in kcal mol^{-1}) for dinuclear species with respect to the monomers. Detected stoichiometries in ESI-MS are $[W_2O_7]^{2-}$, $[Mo_2O_7]^{2-}$ and $[W_2O_6(OH)]^-$ highlighted in boldface type.

Structure			ΔE (kcal mol^{-1})			
			M=W		M=Mo	
			X=P	X=As	X=P	X=As
$[M_2O_6(OH)_2]^{2-}$	**1**	a	–7.5		+0.4	
	2	b	+0.2		+7.4	
	3	c	+10.2		+11.4	
$[M_2O_7]^{2-}$	**1**	d	–4.4		–2.2	
	2	e	–3.3		–2.1	
$[M_2O_6(OH)]^-$	**1**	f	–21.9		–17.9	
$[XMO_5(OH)_3]^{2-}$	**1**	g	+2.4	+1.3	+4.2	+3.7
	2	h	+12.6	+13.2	+15.7	+14.0
	3	i	+3.0	+3.2	+5.5	+8.4
	4	j	+27.3	+10.3	+30.2	+12.9
$[XMO_6(OH)]^{2-}$	**1**	k	+0.8	+2.5	+1.6	+1.76
	2	l	+2.2	+0.6	+1.7	+0.92
	3	m	+1.5	–0.3	+1.5	+0.16
$[XMO_5(OH)_2]^-$	**1**	n	–18.6	–22.2	–17.2	–21.4

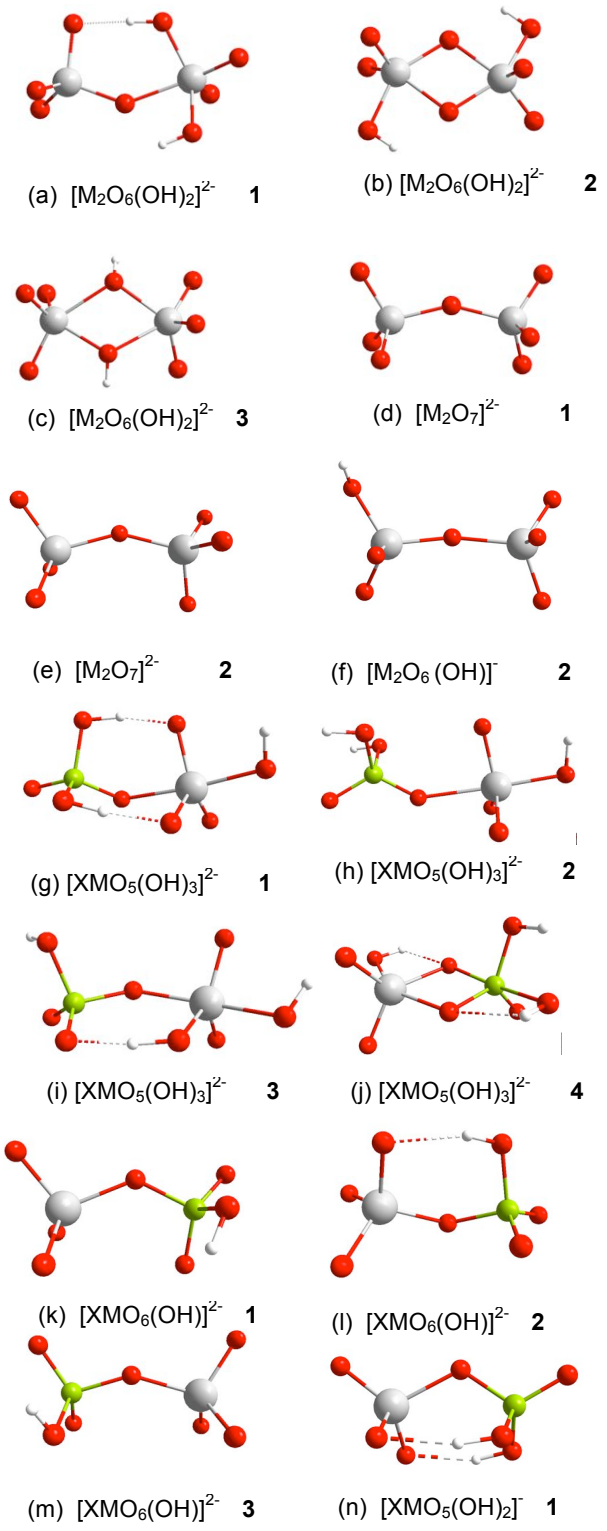

Figure S1. Optimized structures for the most representative dinuclear species.

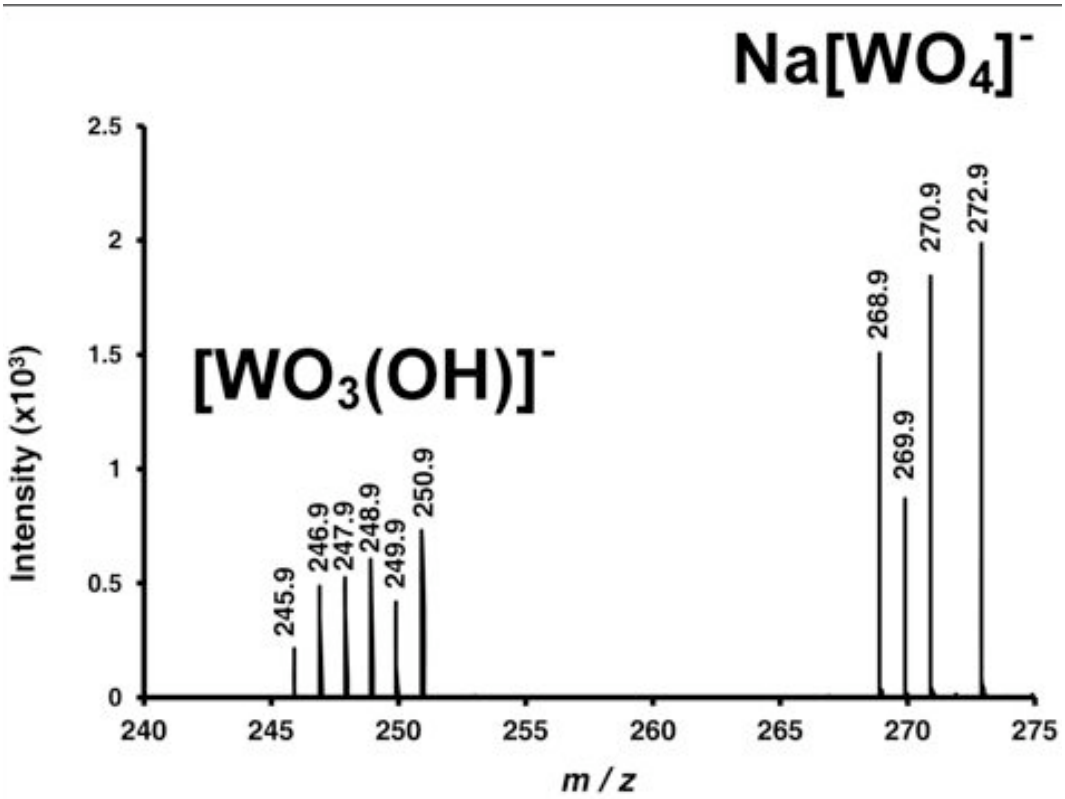

Figure S2. Monomeric fragments $[WO_3(OH)]^-$ (*m/z* 248.9) and $Na[WO_4]^-$ (*m/z* 270.9) observed in the assembly solution of $[(n\text{-}C_4H_9)_4N]_3AsW_{12}O_{40}$ in the Mass Spectrometer.

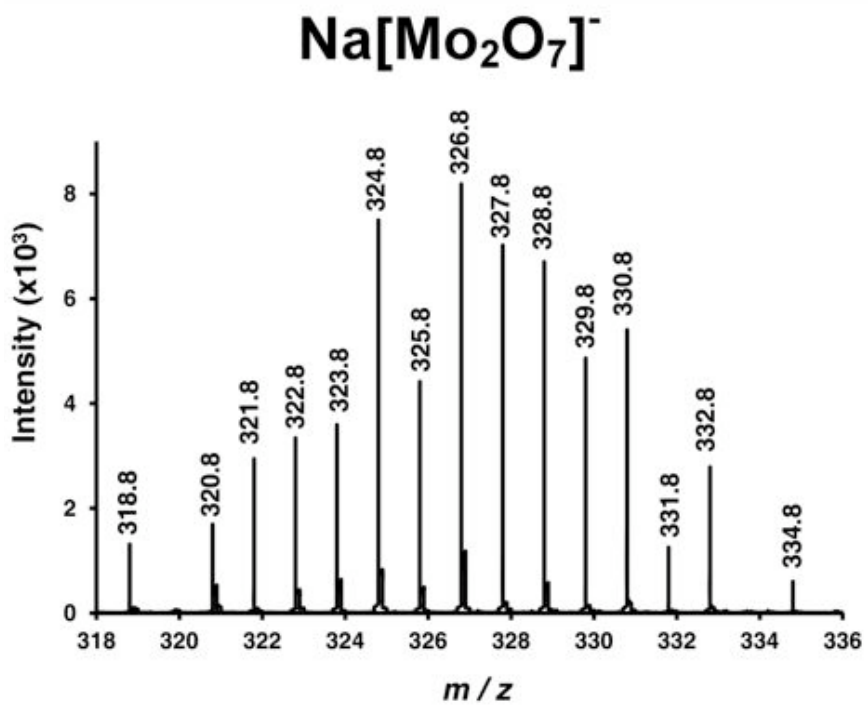

Figure S3. Isodimeric fragment $Na[Mo_2O_7]^-$ (*m/z* 326.8) observed in the assembly solution of $[(n\text{-}C_4H_9)_4N]_3PMo_{12}O_{40}$ in the Mass Spectrometer.

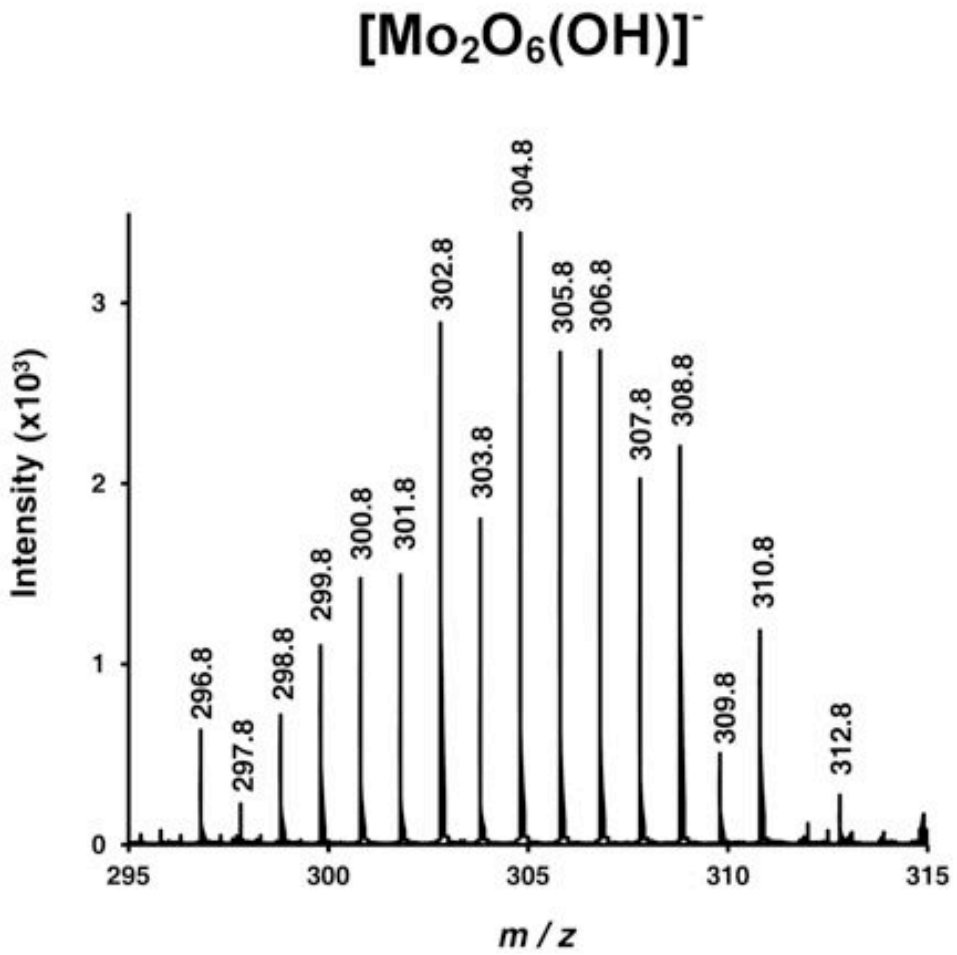

Figure S4. Protonated isodimeric fragment $[Mo_2O_6(OH)]^-$ (*m/z* 304.8) observed in the assembly solution of $[(n\text{-}C_4H_9)_4N]_3PMo_{12}O_{40}$ in the Mass Spectrometer.

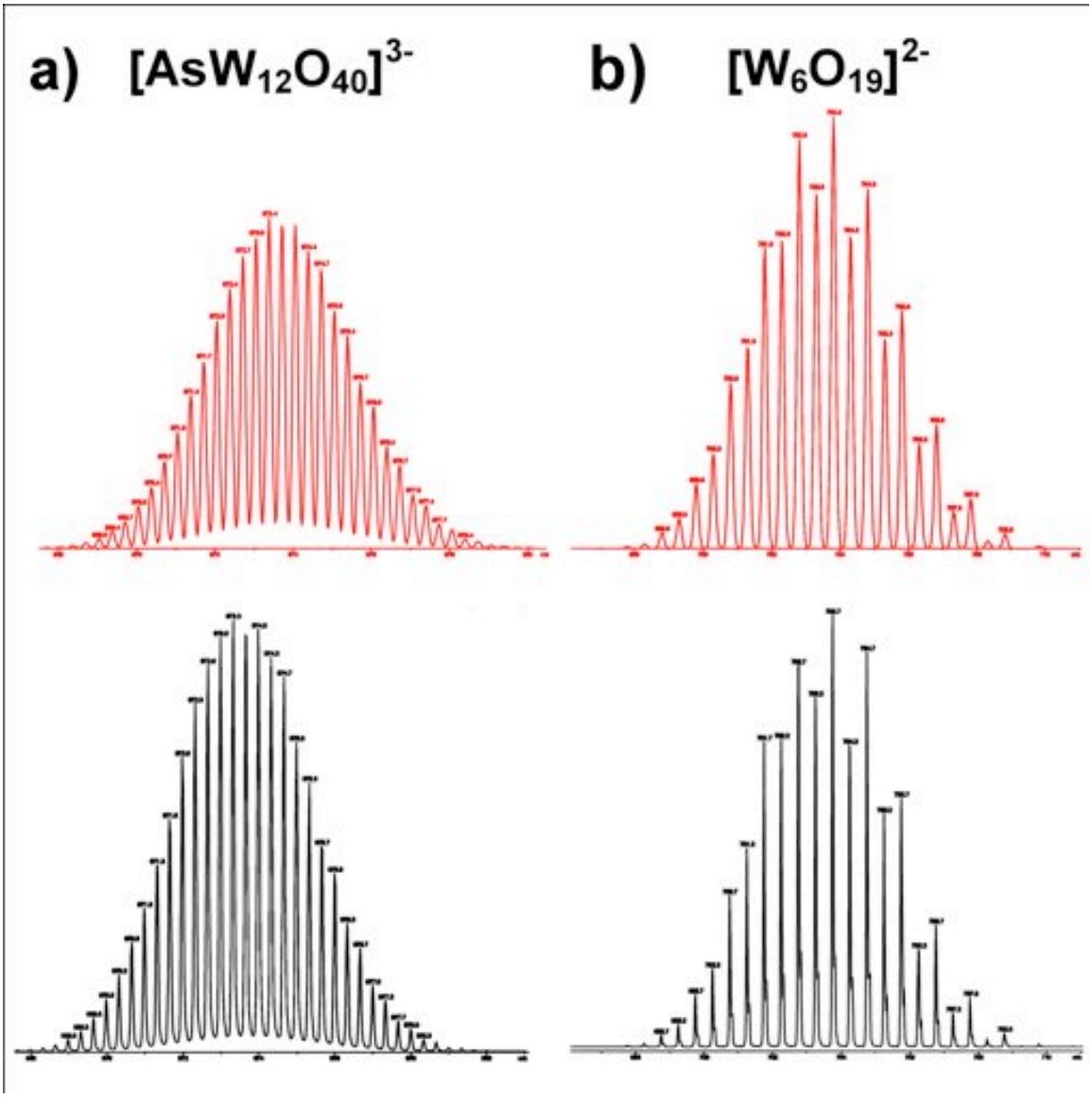

Figure S5. Comparison of experimental (top, red) and theoretical (bottom, black) mass spectra for (a) $[AsW_{12}O_{40}]^{3-}$ (*m/z* 973.3); and (b) $[W_6O_{19}]^{2-}$ (*m/z* 703.8). The experimental (red) isotope patterns shown above for the ion assigned peaks were generated from $[(n\text{-}C_4H_9)_4N]_3AsW_{12}O_{40}$ dissolved in acetonitrile solution and studies by ESI-MS.

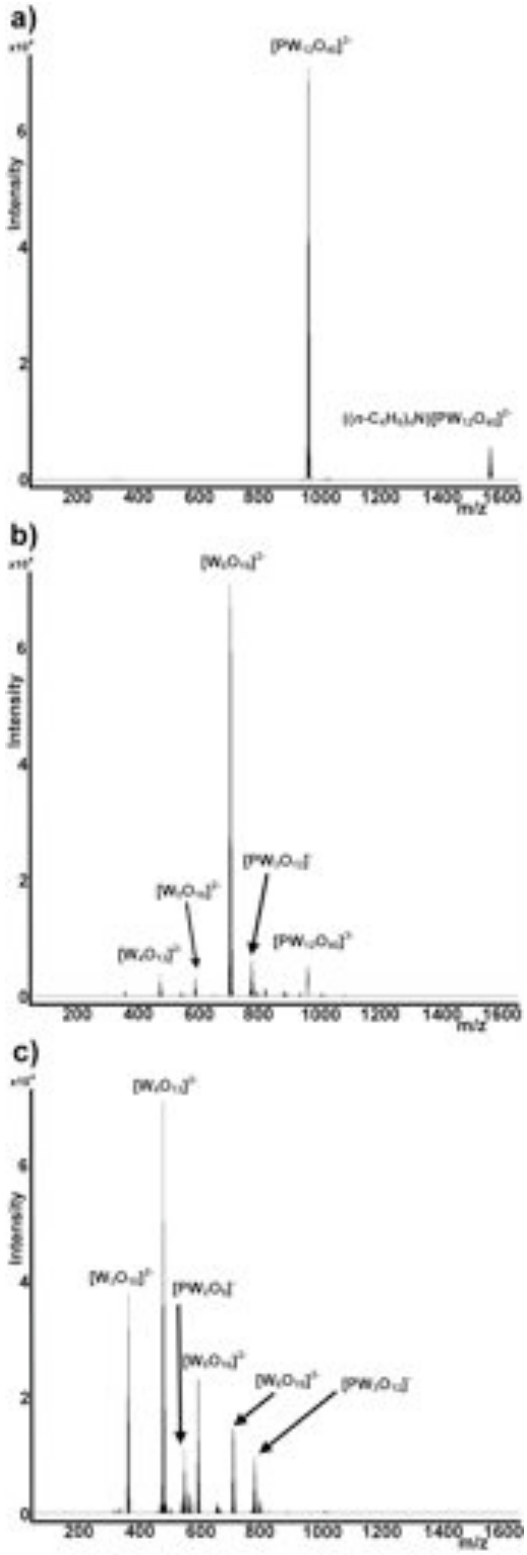

Figure S6. Electrospray Ionisation Mass Spectrometry data showing the collision induced dissociation (CID) of $[(n\text{-}C_4H_9)_4N]_3PW_{12}O_{40}$ in acetonitrile showing the major ions observed in the gas phase at collision energies (CE) a) 5 eV; b) 25 eV; c) 45 eV respectively.

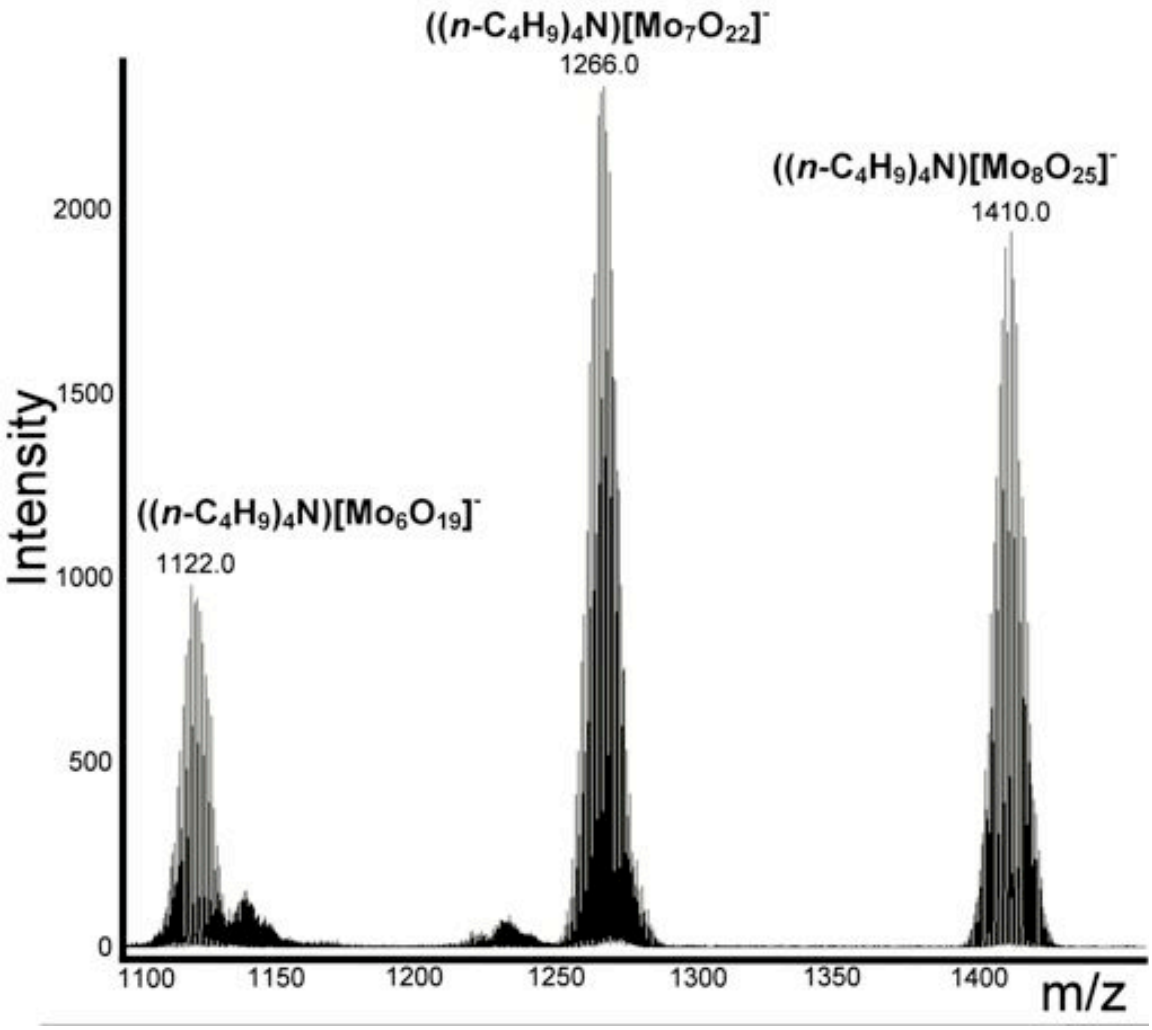

Figure S7. Electrospray Ionisation Mass Spectrometry data of collision induced dissociation (CID) of $[(n\text{-}C_4H_9)_4N]_3AsMo_{12}O_{40}$ in acetonitrile showing the presence of key ions in the gas phase $((n\text{-}C_4H_9)_4N)[Mo_6O_{19}]^-$ (*m/z* 1122.0); $((n\text{-}C_4H_9)_4N)[Mo_7O_{22}]^-$ (*m/z* 1266.0) and $((n\text{-}C_4H_9)_4N)[Mo_8O_{25}]^-$ (*m/z* 1410.0).

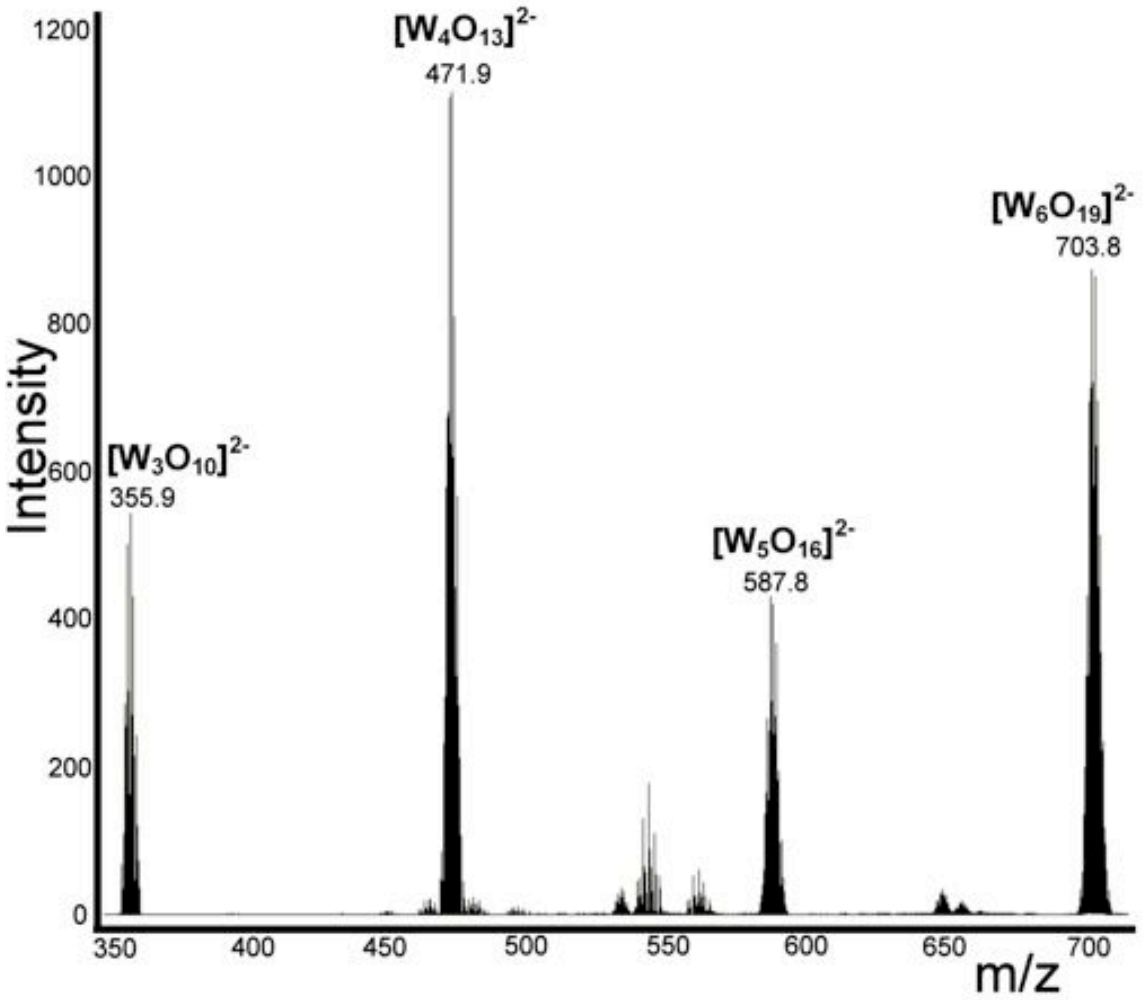

Figure S8. Electrospray Ionisation Mass Spectrometry data of collision induced dissociation (CID) of $[(n\text{-}C_4H_9)_4N]_3PW_{12}O_{40}$ in acetonitrile showing the presence of key doubly charged ions in the gas phase: $[W_3O_{10}]^{2-}$ (*m/z* 355.9); $[W_4O_{13}]^{2-}$ (*m/z* 471.9); $[W_5O_{16}]^{2-}$ (*m/z* 587.8) and $[W_6O_{19}]^{2-}$ (*m/z* 703.8)

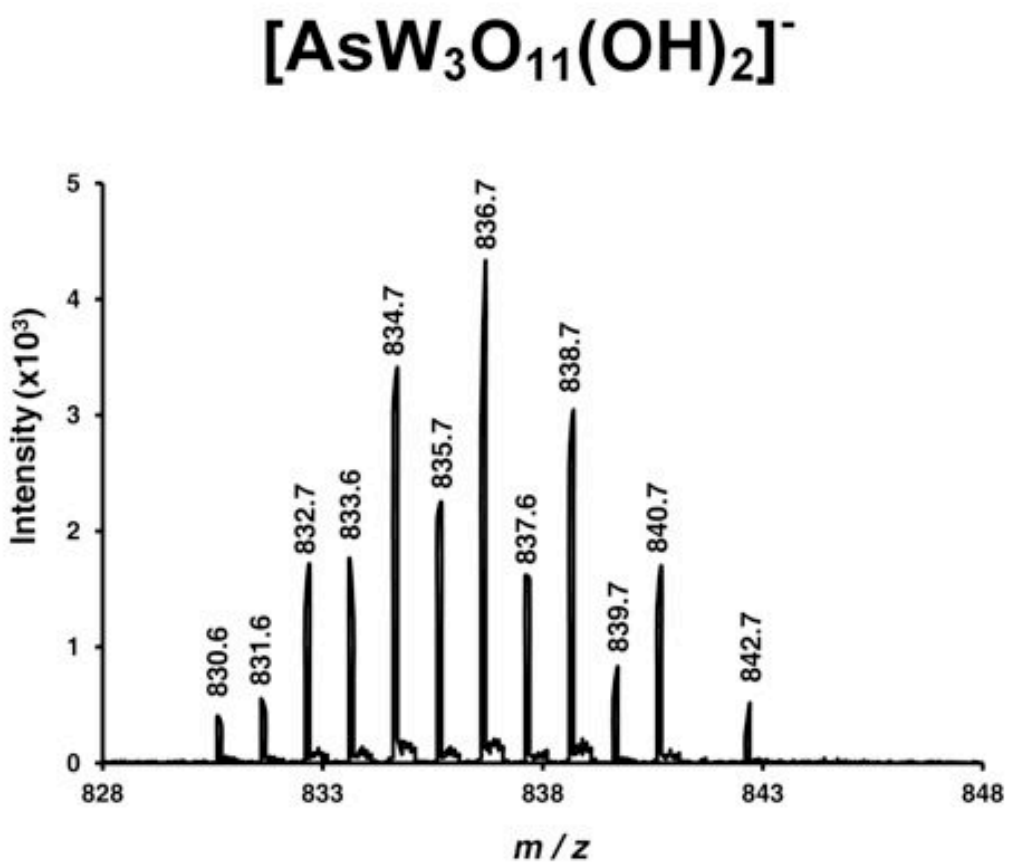

Figure S9. Heterotetrameric fragment $[AsW_3O_{11}(OH)_2]^-$ (*m/z* 836.7) observed in the fragmentation of $[(n\text{-}C_4H_9)_4N]_3AsW_{12}O_{40}$ in acetonitrile.

Table S2. A summary of the common fragments observed in the assembly and fragmentation of Keggin anions, $[XM_{12}O_{40}]^{3-}$ (X = P, As; M = W, Mo), transferred to the gas phase by electrospray ionization and analysed in the Mass Spectrometer.

Nucleation	Assembly		Fragmentation	
	W-Keggins[a]	Mo-Keggins	W-Keggins[a]	Mo-Keggins
Monomer	$Na[WO_4]^-$	$Na[MoO_4]^-$		
	$[WO_3(OH)]^-$	$[MoO_3(OH)]^-$		
Dimer	$Na[W_2O_7]^-$	$Na[Mo_2O_7]^-$		
		$((n\text{-}C_4H_9)_4N)[Mo_2O_7]^-$		
	$[W_2O_6(OH)_2]^{2-}$	$Na[Mo_2O_6(OH)_2]^-$		
		$Li[Mo_2O_6(OH)_2]^-$		
		$[Mo_2O_6(OH)]^-$		
Trimer			$[XW_2O_9]^-$	
			$[XW_2O_8(OH)_2]^-$	
			$[W_3O_{10}]^{2-}$	
Tetramer			$[W_4O_{13}]^{2-}$	$[Mo_4O_{13}]^{2-}$
				$((n\text{-}C_4H_9)_4N)[Mo_4O_{13}]^-$
			$[XW_3O_{12}]^-$	$[XMo_3O_{12}]^-$
			$[XW_3O_{11}(OH)_2]^-$	
Pentamer			$[XW_4O_{15}]^-$	$[XMo_4O_{15}]^-$
			$[W_5O_{16}]^{2-}$	$[Mo_5O_{16}]^{2-}$
Hexamer			$[W_6O_{19}]^{2-}$	$[Mo_6O_{19}]^{2-}$
				$((n\text{-}C_4H_9)_4N)[Mo_6O_{19}]^-$
Heptamer			$[W_7O_{22}]^{2-}$	$[Mo_7O_{22}]^{2-}$
				$((n\text{-}C_4H_9)_4N)[Mo_7O_{22}]^-$
Octamer				$[Mo_8O_{25}]^{2-}$
				$((n\text{-}C_4H_9)_4N)[Mo_8O_{25}]^-$
Dodecamer			$[XW_{12}O_{40}]^{3-}$	$H[PMo_{12}O_{40}]^{2-}$
			$((n\text{-}C_4H_9)_4N)[XW_{12}O_{40}]^{2-}$	$((n\text{-}C_4H_9)_4N)[XMo_{12}O_{40}]^{2-}$
			$((n\text{-}C_4H_9)_4N)_2[XW_{12}O_{40}]^{1-}$	$((n\text{-}C_4H_9)_4N)_2[XMo_{12}O_{40}]^{1-}$

Table S3. A summary of the Mass Spectrometer parameters employed for assembly and fragmentation experiments.

Data Collection		
MS parameter	**Assembly**	**Fragmentation**
Mass Range (*m/z*)	**20 - 1000**	**50 – 5000**
Capilary (V)	**4000**	**4000**
Collision Energy (eV)	**-5**	**-5 to -100**
Collision Cell RF (Vpp)	**500**	**600**
Transfer Time (µs)	**80**	**60-120**
Pre-pulse Storage Time (µs)	**10**	**10**
Summation	**6000**	**6000**
Time of Acquisition (min)	**2**	**2**
Active Focus	**OFF**	**ON**

Table S4. Relative energies, with respect to the most stable geometry, (in kcal mol^{-1}) for $[XM_2O_8(OH)_3]^{2-}$ and $[XM_2O_8(OH)_2]^-$ stoichiometries (in bold, those structures for which harmonic frequencies have been computed). The results are organized with respect the values from stoichiometries $[PW_2O_8(OH)_3]^{2-}$ and $[PW_2O_8(OH)_2]^-$ in order of decreasing stability. Detected stoichiometry in ESI-MS experiment is $[PW_2O_8(OH)_2]^{2-}$ highlighted in boldface type.

Structure			ΔE (kcal mol^{-1})			
			M=W		M=Mo	
			X=P	X=As	X=P	X=As
$[XM_2O_8(OH)_3]^{2-}$	**1**	a	**0.0**	**0.0**	**0.0**	**0.0**
	2	b	**+7.9**	**+3.3**	**+5.2**	-
	3	c	**+8.4**	**+9.3**	**+9.7**	-
	4	d	**+11.4**	**+8.9**	**+9.8**	-
	5	e	**+11.7**	**+7.2**	**+8.6**	**+6.3**
	6	f	**+15.7**	**+7.5**	**+18.8**	-
$[XM_2O_8(OH)_2]^-$	**1**	h	**0.0**	+0.1	**0.0**	**0.0**
	2	i	**+2.9**	**0.0**	+2.2	**+4.8**
	3	j	**+3.4**	**+0.3**	+1.7	+2.9
	4	k	**+4.0**	+1.0*	+1.6	+2.3*
	5	l	**+6.1**	+1.2	+5.7	+4.9

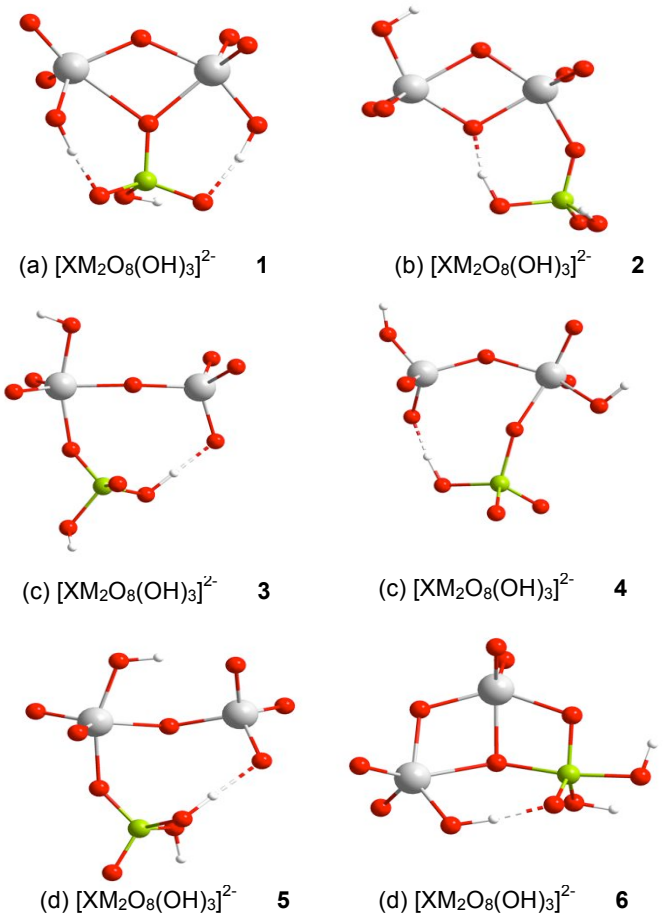

Figure S10. Optimized structures for the most representative trinuclear species. The structures are organized with respect the results of stoichiometry $[PW_2O_8(OH)_3]^{2-}$ in order of decreasing stability.

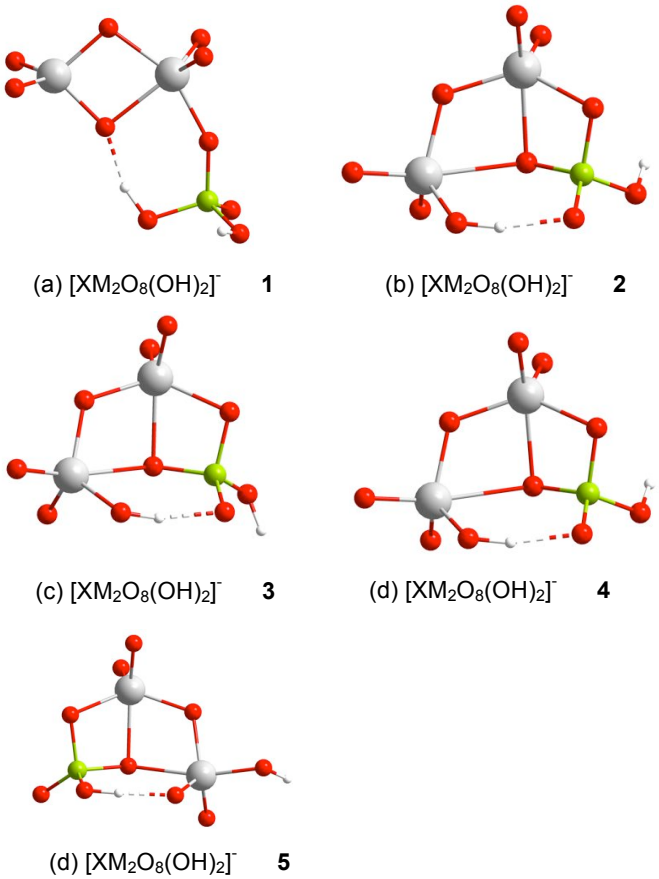

Figure S11. Optimized structures for the most representative trinuclear species. The structures are organized with respect to the results of stoichiometry $[PW_2O_8(OH)_2]^-$ in order of decreasing stability. There are minor geometrical differences between geometries 2 and 4, they are degenerated in energy (~1 Kcal mol^{-1}).

*Optimized structures for the case of structure 5 $[AsM_2O_8(OH)_2]^-$

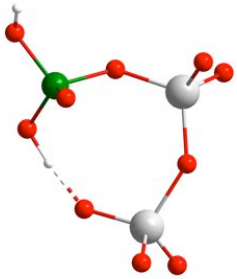

Table S5. Relative energies, with respect to the most stable geometry, (in kcal mol^{-1}) for $[XM_2O_9(OH)_2]^{3-}$ stoichiometry (in bold, those structures for which harmonic frequencies have been computed). The results are organized with respect the results of stoichiometry $[PW_2O_9(OH)_2]^{3-}$ in order of decreasing stability.

Structure			ΔE (kcal mol^{-1})			
			M=W		M=Mo	
			X=P	X=As	X=P	X=As
$[XM_2O_9(OH)_2]^{3-}$	**1**	a	**0.0**	**+0.1**	+2.0	+4.0
	2	b	**+1.1**	**0.0**	+0.6	+3.4
	3	c	**+2.8**	**+1.7**	**0.0**	**0.0**
	4	d	**+4.1**	**0.0**	+9.9	+7.5
	5	e	**+5.5**	+9.7*	+12.2	+11.8*
	6	f	+6.0	+4.4	+10.5	+9.4
	7	g	**+6.2**	**+3.7**	+8.8	+10.1
	8	h	**+6.6**	+3.9	-	-
	9	i	**+7.0**	+9.8	-	-
	10	j	+8.6	+3.0	-	-
	11	k	+9.5	+10.1	-	-
	12	l	+9.6	+8.2	-	-
	13	m	+9.8	+9.4	-	-
	14	n	**+10.2**	+7.0	-	-
	15	o	**+10.3**	+15.3	-	-
	16	p	+28.0	-	-	-

*Optimized structures for the case of structure 5 $[AsM_2O_9(OH)_2]^{3-}$

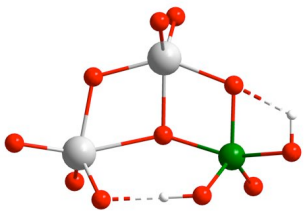

(e) $[AsM_2O_9(OH)_2]^{3-}$ **5**

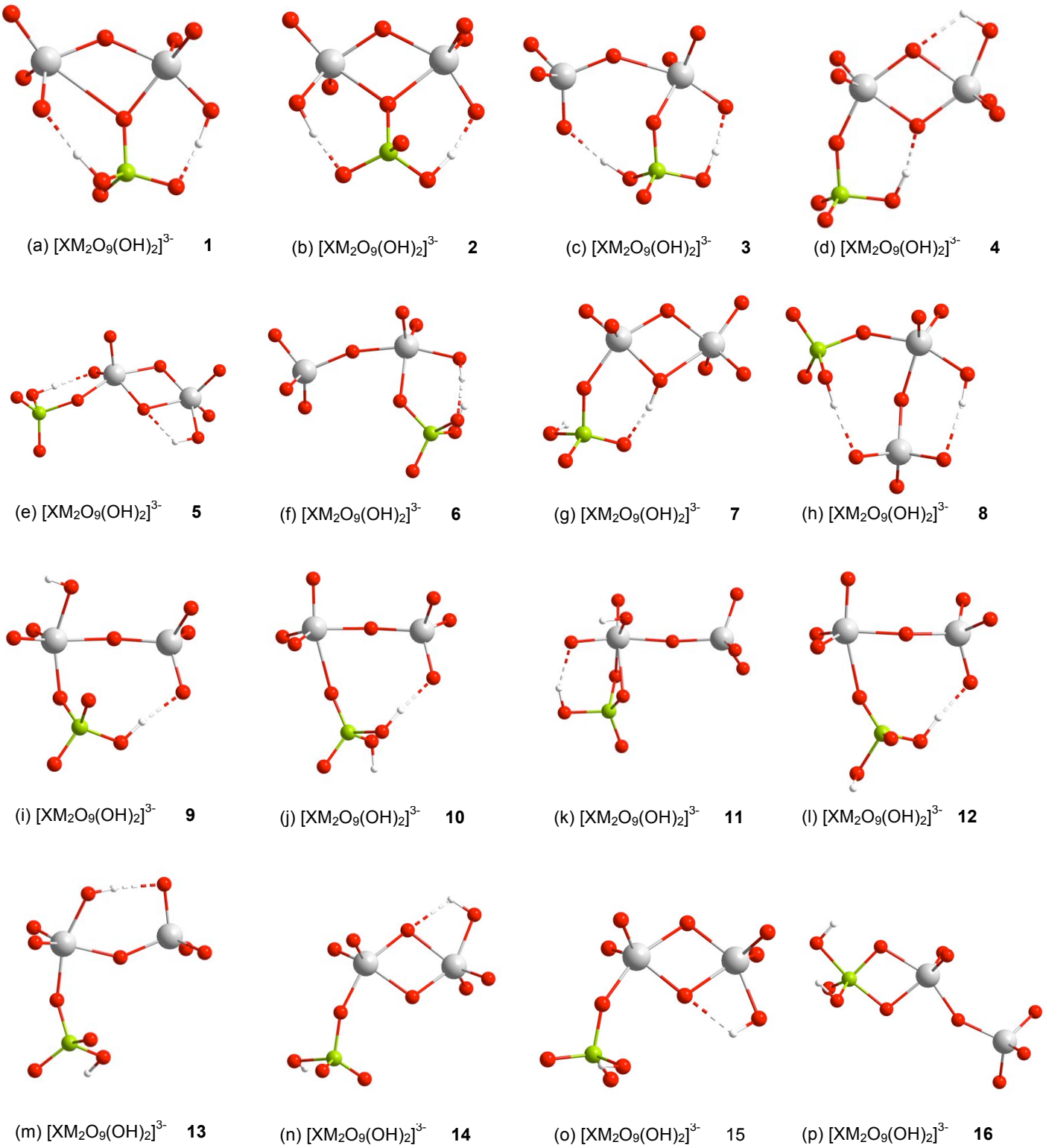

Figure S12. Optimized structures for the most representative trinuclear species. The structures are organized with respect the results of stoichiometry $[PW_2O_9(OH)_2]^{3-}$ in order of decreasing stability

Table S6. Relative energies, with respect to the most stable geometry, (in kcal mol^{-1}) for $[XM_2O_9OH)]^{2-}$ and $[XM_2O_9]^-$ stoichiometries (in bold, those structures for which harmonic frequencies have been computed). Detected stoichiometries in ESI-MS experiment are $[PW_2O_9]^-$ and $[AsW_2O_9]^-$, highlighted in boldface type.

Structure			ΔE (kcal mol^{-1})			
			M=W		M=Mo	
			X=P	X=As	X=P	X=As
$[XM_2O_9(OH)]^{2-}$	**1**	a	**0.0**	+3.5	+1.5	+6.1
	2	b	**+0.6**	**0.0**	**0.0**	**0.0**
	3	c	+1.4	+2.4	+3.0	+1.1
	4	d	+2.6	+12.5	+4.6	+9.7
	5	e	+3.3	+2.9	+1.3	+1.3
	6	f	+4.6	+1.9	+5.8	+0.7
	7	g	+8.2	+9.7	+7.4	+8.5
	8	h	+11.3	+7.0	+12.6	+0.9
$[XM_2O_9]^-$	**1**	g	**0.0**	+4.7	**0.0**	+7.8
	2	h	**+3.9**	**0.0**	**+0.3**	**0.0**
	3	i	+4.1	+3.2	+4.8	+6.5
	4	j	+6.5	+1.0	+5.7	+2.3
	5	k	+18.3	+12.4	+16.7	+14.3
	6	l	+37.0	+20.3	+34.4	+23.3

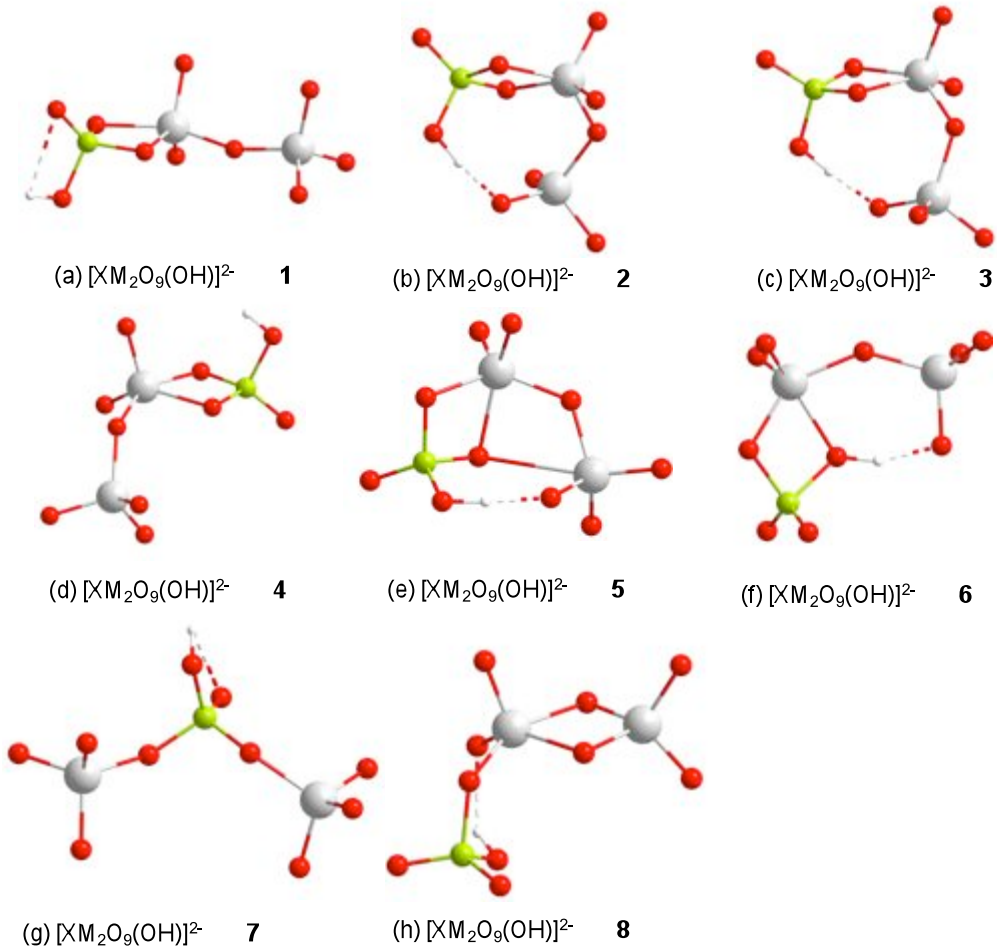

Figure S13. Optimized structures for the most representative trinuclear species. The structures organized with respect the results of stoichiometry $[PW_2O_9(OH)]^{2-}$ in order of decreasing stability. Structures 1 and 2 are practically degenerated.

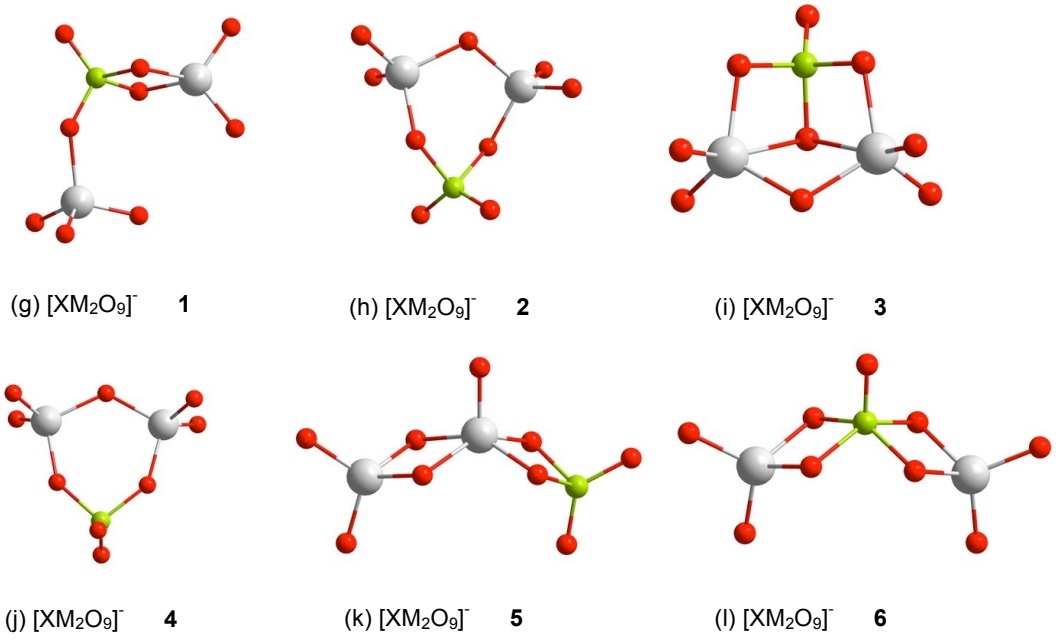

Figure S14. Optimized structures for the most representative trinuclear species. The structures organized with respect the results of stoichiometry $[PW_2O_9]^-$ in order of decreasing stability.

Table S7. Relative energies, with respect to the most stable geometry, (in kcal mol^{-1}) for $[XM_3O_{11}(OH)_3]^{2-}$ stoichiometry (in bold, those structures for which harmonic frequencies have been computed). Geometry 4 is a triad-Keggin like structure.

Structure			ΔE (kcal mol^{-1})	
			M=W	
			X=P	X=As
$[XM_3O_{11}(OH)_3]^{2-}$	**1**	a	**0.0**	**0.0**
	2	b	+12.6	+19.5
	3	c	+14.8	+15.8
	4	d	+16.4	+19.1
	5	e	+20.7	-
	6	f	+23.5	-
	7	g	+23.7	-
	8	h	+24.0	-
	9	i	+24.8	-
	10	j	+25.7	-
	11	k	+26.0	-
	12	l	+27.2	

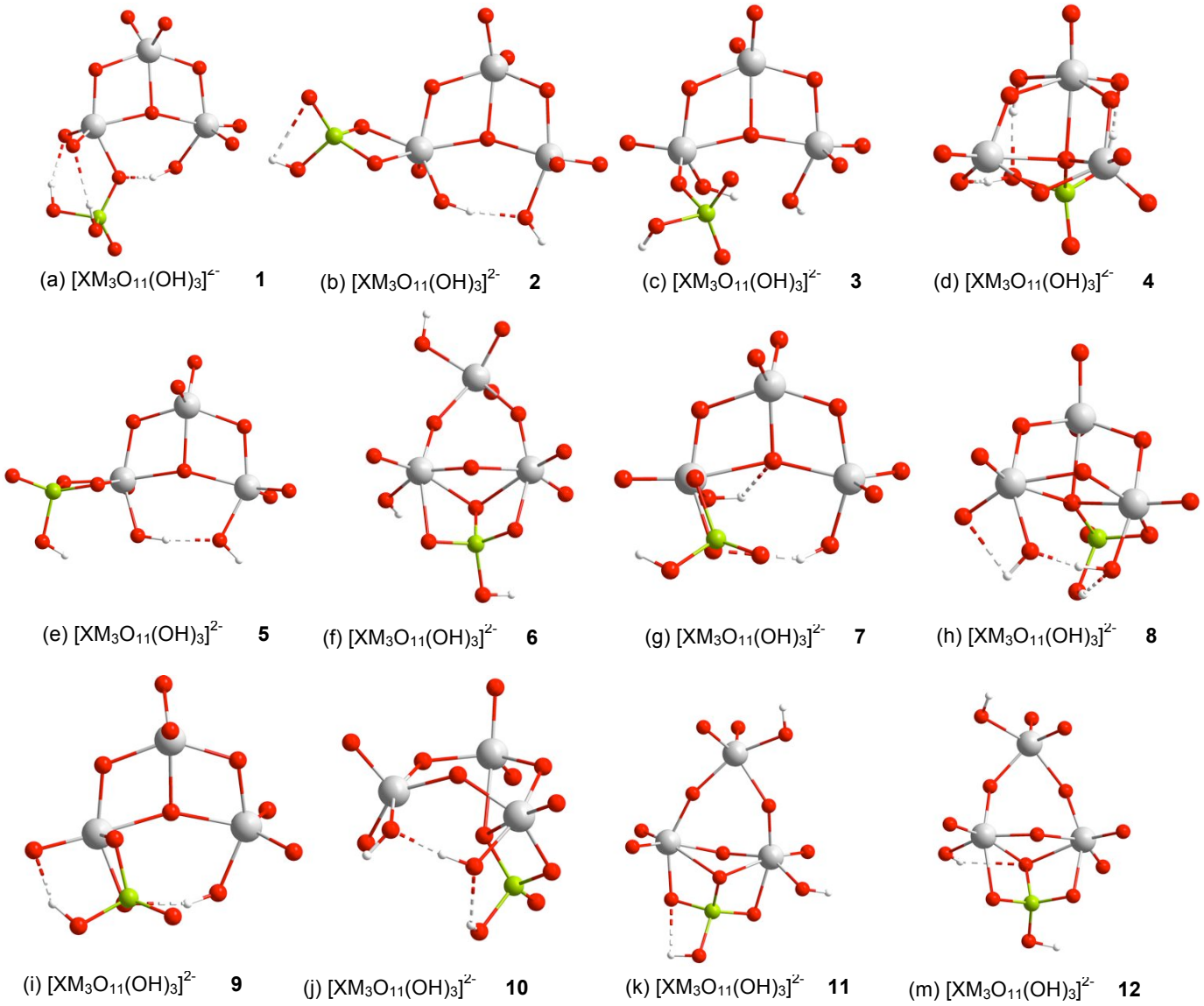

Figure S15. Optimized structures for $[XM_3O_{11}(OH)_3]^{2-}$ stoichiometry. The structures are organized in order of decreasing stability.

Table S8. Relative energies, with respect to the most stable geometry, (in kcal mol^{-1}) for $[XM_3O_{11}(OH)_2]^-$ stoichiometry (in bold, those structures for which harmonic frequencies have been computed). Detected stoichiometries in ESI-MS experiment are $[PW_3O_{11}(OH)_2]^-$ and $[AsW_3O_{11}(OH)_2]^-$, highlighted in boldface type.

Structure			ΔE (kcal mol^{-1})	
			M=W	
			X=P	X=As
$[XM_3O_{11}(OH)_2]^-$	**1**	a	**0.0**	**0.0**
	2	b	**+4.2**	+0.6
	3	c	+4.3	+5.5
	4	d	+6.4	+10.1
	5	e	+7.5	-
	6	f	+15.8	-
	7	g	+15.9	-
	8	h	+15.9	-
	9	i	+16.3	-
	10	j	+16.7	-
	11	k	+17.7	-
	12	l	+20.6	-
	13	m	+50.1	-

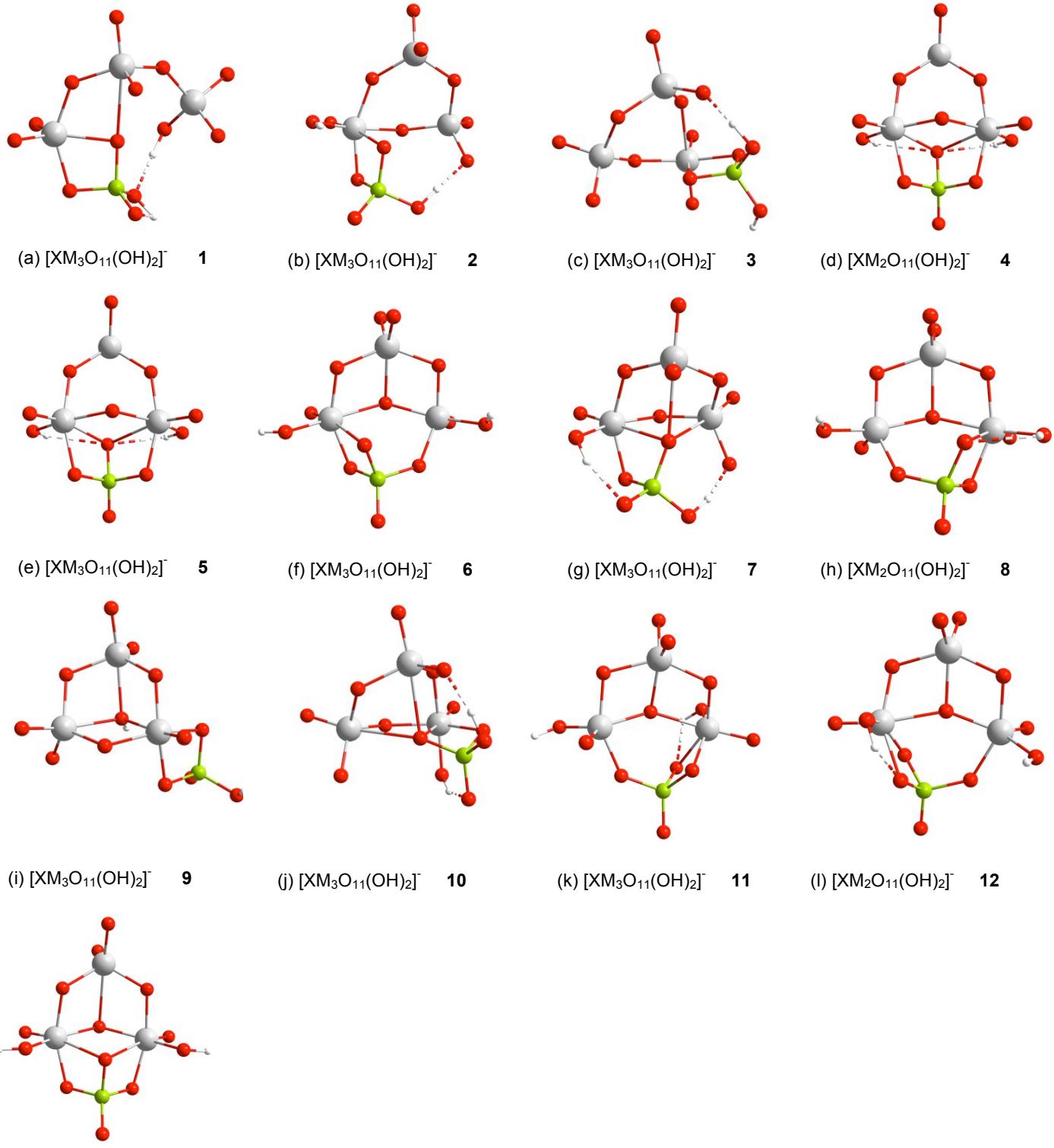

Figure S16. Optimized structures for $[XM_3O_{11}(OH)_2]^-$ stoichiometry. The structures are organized in order of decreasing stability.

Table S9. Relative energies, with respect to the most stable geometry, (in kcal mol^{-1}) for $[XM_3O_{12}(OH)]^{2-}$ stoichiometry (in bold, those structures for which harmonic frequencies have been computed).

Structure			ΔE (kcal mol^{-1})	
			M=W	
			X=P	X=As
$[XM_3O_{12}(OH)]^{2-}$	**1**	**a**	**0.0**	**0.0**
	2	b	+0.4	+2.5
	3	c	+0.4	+2.8
	4	d	+1.0	+4.2
	5	e	+1.2	+3.7
	6	f	+13.0	-
	7	g	+13.7	-
	8	h	+14.9	-
	9	i	+15.7	-

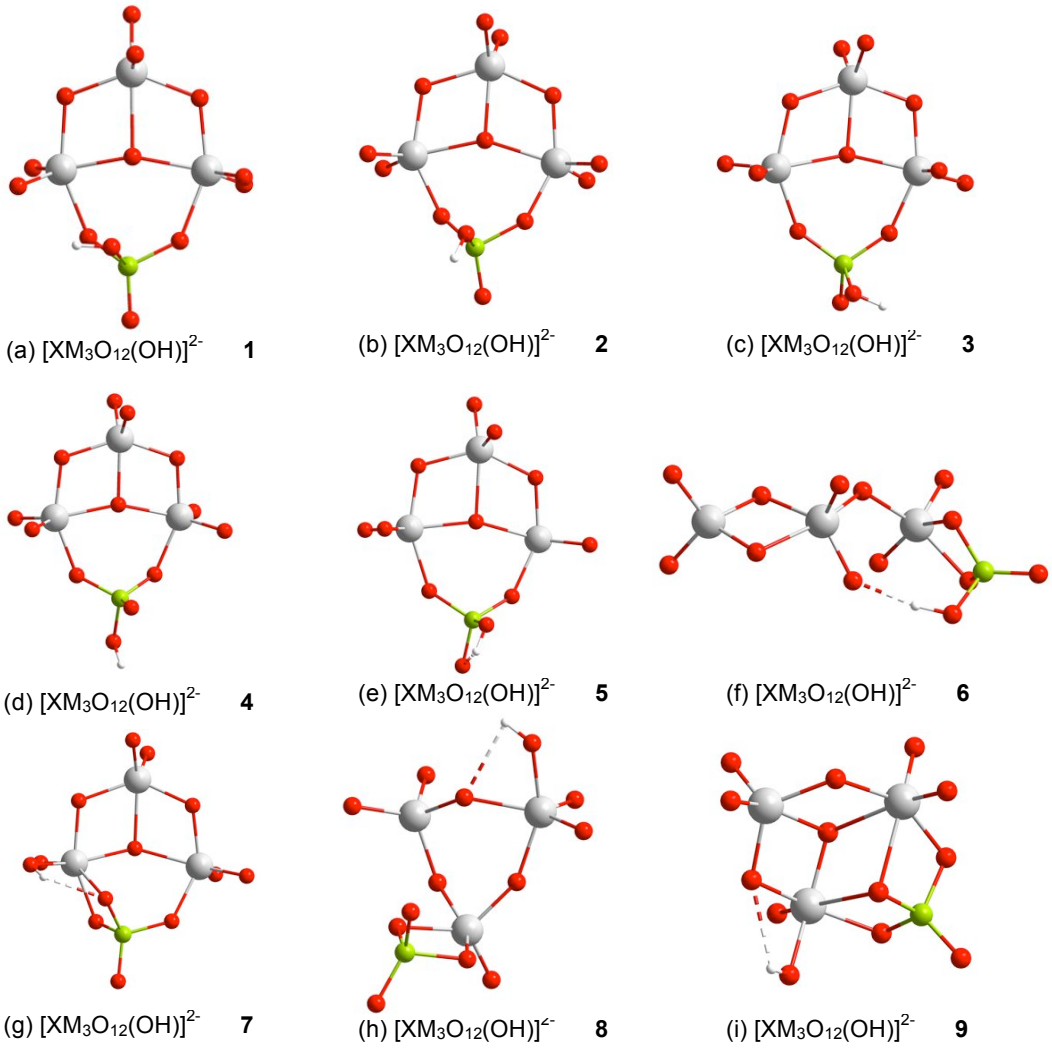

Figure S17. Optimized structures for $[XM_3O_{12}(OH)]^{2-}$ stoichiometry. The structures are organized in order of decreasing stability.

Table S10. Relative energies, with respect to the most stable geometry, (in kcal mol^{-1}) for $[XM_3O_{12}]^-$ stoichiometry (in bold, those structures for which harmonic frequencies have been computed). Detected stoichiometries in ESI-MS experiment are $[PM_3O_{12}]^-$ and $[AsM_3O_{12}]^-$, highlighted in boldface type.

Structure			ΔE (kcal mol^{-1})	
			M=W	
			X=P	X=As
$[XM_3O_{12}]^-$	**1**	a	**0.0**	**0.0**
	2	b	+4.0	+5.1
	3	c	**+6.5**	+9.5
	4	d	**+6.8**	+6.1
	5	e	**+8.6**	-
	6	f	**+11.0**	-
	7	g	**+12.4**	-
	8	h	**+12.6**	-
	9	i	**+13.3**	-
	10	j	+13.6	-
	11	k	+14.0	-
	12	l	**+31.0**	-
	13	m	+38.7	-

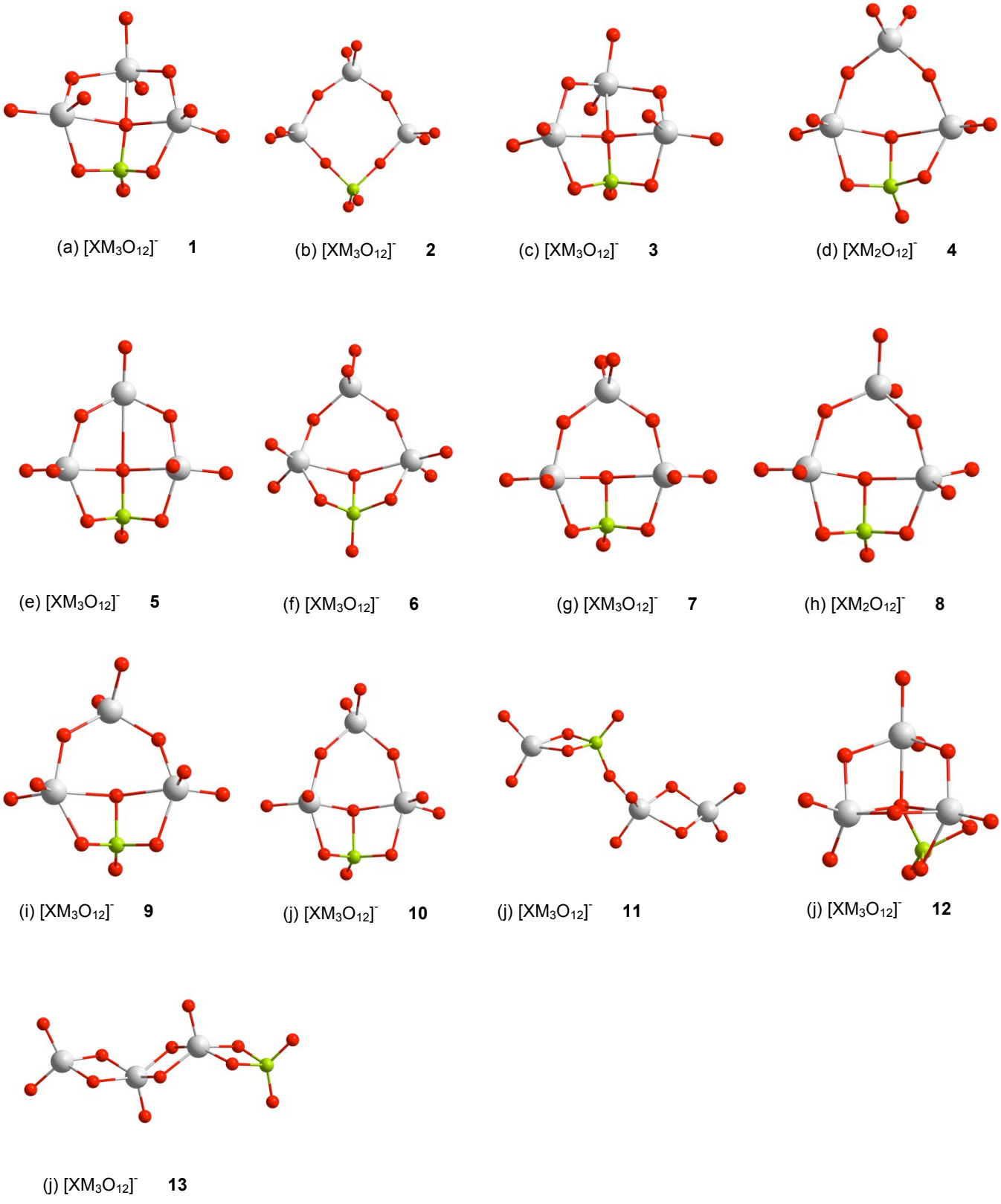

Figure S18. Optimized structures for $[XM_3O_{12}]^-$ stoichiometry. The structures are organized in order of decreasing stability

Experimental Section:

Fragmentation experiments

Tetra-*n*-butylammonium salts (TBA = [(n-C_4H_9)$_4$N]) of these Keggin anions were prepared by the following method: 1 mol of the relevant Keggin anion was dissolved in water and to it added 10 mol of Tetra-*n*-butylammonium bromide (TBABr). The resulting precipitate was allowed to stir for 10 min and subsequently filtered by Büchner filtration. The solid products were then washed twice by the following: water, ethanol and diethyl ether before being dried *in vacuo*. Purification of the TBA-Keggin salts was achieved by solubilizing small quantities of the TBA-salts in acetonitrile and setting up a diethyl ether vapour diffusion crystal growth method. Single crystals of the TBA-Keggin salts appear in the acetonitrile solution within several hours.

Elemental analysis (%) calcd. for ((n-C_4H_9)$_4$N)$_3$[$PMo_{12}O_{40}$], $C_{48}H_{108}Mo_{12}N_3O_{40}P$ (2573.0 g mol^{-1}): C 22.39, H 4.20, N 1.63; found (%):C 22.63, H 4.21, N 1.95. Elemental analysis (%) calcd. for ((n-C_4H_9)$_4$N)$_3$[$PW_{12}O_{40}$], $C_{48}H_{108}W_{12}N_3O_{40}P$ (3605.0 g mol^{-1}): C 15.98, H 3.00, N 1.17; found (%):C 15.89, H 2.96, N 1.23. Elemental analysis (%) calcd for ((n-C_4H_9)$_4$N)$_3$[$AsMo_{12}O_{40}$], $C_{48}H_{108}Mo_{12}N_3O_{40}As$ (2617.0 g mol^{-1}): C 22.00, H 4.13, N 1.60; found (%):C 22.80, H 4.26, N 1.86. Elemental analysis (%) calcd. for ((n-C_4H_9)$_4$N)$_3$[$AsW_{12}O_{40}$], $C_{48}H_{108}W_{12}N_3O_{40}As$ (3649.0 g mol^{-1}): C 15.79, H 2.96, N 1.15; found (%):C 15.77, H 2.98, N 1.14.

Computational methodology

COSMO methodology: To define the cavity that surrounds the molecules we use the solvent accessible surface (SAS) method and a fine tesserae. Once the geometry has been optimized using the SAS surface, we perform single-point calculations using the solvent excluding surface (SES) that yields more meaningful values for the hydration energies. Geometry optimization using the SES yields “unrealistic” distorted structures when the coordination number of W(VI) ions is lower than six. To obtain the electron density in solution, first it is converged in the gas phase and afterward the COSMO model is turned on to include the solvent effects variationally. The ionic radii of the atoms, which define the dimensions of the cavity surrounding the molecule, are chosen to be 1.26 Å for W, 0.64 for Mo, 1.52 for O, 1.00 for P, 0.56 for As and 1.20 for H.

Harmonic frequencies have been computed for most of the structures analyzed through this work: (i) All iso- and heterodinuclear species in Table S1 and Figure S1; (ii) All heterotrinuclear structures shown in Fig. 8 and most of the structures in Tables S4-S6 (those with energies highlighted in bold); (iii) All heterotetranuclear structures shown in Fig. 10 and many structures in Tables S7-S10 (those with energies highlighted in bold). In almost all the cases, the structures correspond to minima in the potential energy surface (all frequencies are positive). For some structures, one o few more imaginary frequencies with tiny values (absolute values smaller than 100 cm^{-1}) are obtained. All these small imaginary frequencies, which are probably due to errors in the numerical calculation of the frequencies (these stationary points could be also considered as minima within the numerical error), correspond to modes in which the H atoms are involved. No displacements of the M or O atoms of the POM framework were detected.

No imaginary frequencies are found corresponding to modes that involve the M, X or O atoms. Since the number of computed structures is very large, we have decided to not incorporate them here. Anyone interested in these values can contact us and we will provide them.

Estimation of free energies from BP86/TZP/COSMO calculations: The reaction free energies have been computed within the harmonic approximation. Since the reaction takes place in solution, we have only considered the thermal and entropic vibrational contributions (translational and rotational contributions might probably be similar for reactants and products due to the large number of molecules in the condensed phase). As shown in Tables S11-S13, reaction free energies show the same trends as reaction energies, leading to the same main conclusions. In general, formation of products is somewhat more favoured when thermal and entropic effects are considered.

Metadynamics: The metadynamics simulations are based on the selection of collective variables (CV) that are suitable to describe the process. The parameters used in the metadynamics are the following: (i) for the dinuclear system ($[WO_3(OH)]^-$, $[PO_2(OH)_2]^-$, 27 H_2O) k = 1.0 a.u., M = 20.0 a.m.u. The height of the hills (W) is 0.063 kcal·mol^{-1}, their perpendicular width ($\Delta s^{\perp}$) 0.04, and the deposition rate (Δt) 0.0144 ps. The total simulation time (t_{total}) was 20 ps; (ii) Same parameters as previous metadynamics, but W = 0.31 kcal·mol^{-1}; (iii) CV: W···O distance (O from the phosphate group), k = 1.0 a.u., M = 10.0 a.m.u., W = 0.063 kcal·mol^{-1}, $\Delta s^{\perp}$= 0.08, Δt = 0.0144 ps, t_{total} = 33 ps; iv) for the heterotrinuclear system ($[W_2O_6(OH)]^-$, $[PO_2(OH)_2]^-$, 58 H_2O) k= 1.5 a.u., M = 40.0 a.m.u., W = 0.13 kcal·mol^{-1}, $\Delta s^{\perp}$= 0.03, Δt = 0.0144 ps, t_{total} = 30 ps; v) for the isotrinuclear system ($[W_2O_6(OH)]^-$, $[WO_3(OH)]^-$, 58 H_2O) two CVs were used: 1) the coordination number of W from the dimer with respect to the O atoms of the monomer; and 2) the coordination number of W from the monomer with respect to the O atoms of the dimer; $k_1 = k_2$ = 1.5 a.u., $M_1 = M_2$ = 40.0 a.m.u., W = 0.31 kcal·mol^{-1}, $\Delta s^{\perp}$= 0.04, Δt =0.0144 ps, t_{total} = 70 ps. The free energy for the first step of the reaction (step 1, Table 1) computed from the metadynamics run matches fairly well (–9 kcal mol^{-1}, ref. 11a) with the estimated value from static BP86/COSMO methodology (–8 kcal mol^{-1}).

Table S11. Energetics associated to the dimer formation.[a,b]

Step	M = W and X = P	ΔE	ΔG	Process type
	Isodimer			
1	$\mathbf{[MO_3(OH)]^-_{(aq)}} + [MO_3(OH)]^-_{(aq)} \rightarrow \mathbf{[M_2O_6(OH)_2]^{2-}_{(aq)}}$	–7.4	–8.3	Aggregation
2a	$\mathbf{[M_2O_6(OH)_2]^{2-}_{(aq)}} \rightarrow \mathbf{[M_2O_7]^{2-}_{(aq)}} + H_2O_{(aq)}$	+2.1	–0.4	Water condensation
2b	$\mathbf{[M_2O_6(OH)_2]^{2-}_{(aq)}} + H_3O^+_{(aq)} \rightarrow \mathbf{[M_2O_6(OH)]^-_{(aq)}} + 2H_2O_{(aq)}$	–14.4	–19.9	Water condensation
	Heterodimer			
1’	$\mathbf{[MO_3(OH)]^-_{(aq)}} + [XO_2(OH)_2]^-_{(aq)} \rightarrow [XMO_5(OH)_3]^{2-}_{(aq)}$	+2.4	+1.0	Aggregation
2a’	$[XMO_5(OH)_3]^{2-}_{(aq)} \rightarrow [XMO_6(OH)]^{2-}_{(aq)} + H_2O_{(aq)}$	–1.6	–3.1	Water condensation
2b’	$[XMO_5(OH)_3]^{2-}_{(aq)} + H_3O^+_{(aq)} \rightarrow [XMO_5(OH)_2]^-_{(aq)} + H_2O_{(aq)}$	–21.0	–23.9	Water condensation

[a] Reaction energies are in kcal mol^{-1}. [b] The species detected in ESI-MS experiments are highlighted in bold.

Table S12. Energetics associated to the trimer formation.[a,b]

Step	M = W and X = P	ΔE	ΔG	Process type
3a	$\mathbf{[M_2O_7]^{2-}_{(aq)}} + [XO_2(OH)_2]^-_{(aq)} \rightarrow [XM_2O_9(OH)_2]^{3-}_{(aq)}$	+1.3	+0.1	Aggregation
4a-1	$[XM_2O_9(OH)_2]^{3-}_{(aq)} + H_3O^+_{(aq)} \rightarrow [XM_2O_9(OH)]^{2-}_{(aq)} + 2H_2O_{(aq)}$	–18.4	–21.5	Water condensation
4a-2	$[XM_2O_9(OH)]^{2-}_{(aq)} + H_3O^+_{(aq)} \rightarrow \mathbf{[XM_2O_9]^-_{(aq)}} + 2H_2O_{(aq)}$	+4.5	0.0	Water condensation
3b	$\mathbf{[M_2O_6(OH)]^-_{(aq)}} + [XO_2(OH)_2]^-_{(aq)} \rightarrow [XM_2O_8(OH)_3]^{2-}_{(aq)}$	–16.9	–16.5	Aggregation
4b	$[XM_2O_8(OH)_3]^{2-}_{(aq)} + H_3O^+_{(aq)} \rightarrow \mathbf{[XM_2O_8(OH)_2]^-_{(aq)}} + 2H_2O_{(aq)}$	+1.8	–2.0	Water condensation

[a] Reaction energies are in kcal mol^{-1}. [b] The species detected in ESI-MS experiments are highlighted in bold.

Table S13. Energetics associated to the tetramer formation.[a,b]

Step	M = W and X = P	ΔE	ΔG	Process type
5a	$\mathbf{[XM_2O_9]^-_{(aq)}} + [MO_3(OH)]^-_{(aq)} \rightarrow [XM_3O_{12}(OH)]^{2-}_{(aq)}$	–31.6	–31.4	Aggregation
6a	$[XM_3O_{12}(OH)]^{2-}_{(aq)} + H_3O^+_{(aq)} \rightarrow \mathbf{[XM_3O_{12}]^-_{(aq)}} + 2H_2O_{(aq)}$	+1.0	–5.3	Water condensation
5b	$\mathbf{[XM_2O_8(OH)_2]^-_{(aq)}} + [MO_3(OH)]^-_{(aq)} \rightarrow [XM_3O_{11}(OH)_3]^{2-}_{(aq)}$	–20.2	–21.4	Aggregation
6b	$[XM_3O_{11}(OH)_3]^{2-}_{(aq)} + H_3O^+_{(aq)} \rightarrow \mathbf{[XM_3O_{11}(OH)_2]^-_{(aq)}} + 2H_2O_{(aq)}$	+6.7	–0.6	Water condensation

[a] Reaction energies are in kcal mol^{-1}. [b] The species detected in ESI-MS experiments are highlighted in bold.